# Selenoprotein P-mediated reductive stress impairs cold-induced thermogenesis in brown fat

**Swe Mar Oo**
Department of Endocrinology and Metabolism, Kanazawa University Graduate School of Medical Sciences

**Hein Ko Oo**
Kanazawa University Graduate School of Medical Sciences https://orcid.org/0000-0003-1155-9080

**Hiroaki Takayama**
Department of Endocrinology and Metabolism, Kanazawa University Graduate School of Medical Sciences

**Takehiro Kanamori**
Department of Endocrinology and Metabolism, Kanazawa University Graduate School of Medical Sciences

**Yumie Takeshita**
Department of Endocrinology and Metabolism, Kanazawa University Graduate School of Medical Sciences

**Kiyo-aki Ishii**
Department of Endocrinology and Metabolism, Kanazawa University Graduate School of Medical Sciences

**Yoshiro Saito**
Tohoku University https://orcid.org/0000-0002-0559-5889

**Mami Matsushita**
Department of Nutrition, Tenshi College

**Yuko Okamatsu-Ogura**
Department of Biomedical Sciences, Graduate School of Veterinary Medicine, Hokkaido University

**Masayuki Saito**
Department of Biomedical Sciences, Graduate School of Veterinary Medicine, Hokkaido University

**Toshinari Takamura** ( ttakamura@med.kanazawa-u.ac.jp )
Kanazawa University Graduate School of Medical Sciences https://orcid.org/0000-0002-4393-3244

---

**Article**

**Keywords:** obesity, diabetes, metabolism

**Posted Date:** February 9th, 2021

**DOI:** https://doi.org/10.21203/rs.3.rs-155060/v1

# Abstract

Reactive oxygen species (ROS) oxidize and activate the uncoupler protein 1 (UCP1) in brown adipose tissue (BAT) under physiological cold exposure and noradrenaline (NA) stimulation to increase thermogenesis. However, pathological significance and the endogenous regulator of the ROS-mediated BAT activation remain unclear.

Here, we show that serum levels of selenoprotein P (SeP, encoded by *Selenop*) are negatively correlated with BAT activity in humans. SeP impairs UCP1 activity and thermogenesis. Physiological cold exposure downregulates *Selenop* in BAT. BAT-specific *Selenop*-deficient (BAT-*Selenop* KO) mice presented elevated NA-induced mitochondrial ROS production, sulfenylated UCP1, and enhanced thermogenesis and glucose uptake in BAT during cold exposure. SeP inhibits mitochondrial ROS by upregulating the expression of the antioxidant enzyme, glutathione peroxidase 4, and impairs glucose uptake in brown adipocytes. High fat/high sucrose diet upregulates *Selenop* in the liver and inhibits the NA-induced BAT thermogenesis in BAT-*Selenop* KO mice.

Our data indicate that SeP, as the hepatokine and BATkine, is the first identified intrinsic factor inducing reductive stress that impairs UCP1 activation and thermogenesis in BAT, and therefore may be a potential therapeutic target for obesity and diabetes.


# Introduction

Converting excess energy to heat in the brown adipose tissue (BAT) will undoubtedly be an attractive solution to obesity and diabetes[1,2]. After a long-standing prevailing belief of BAT existing only in neonates and small rodents, the unexpected evidence of active BAT in adult humans[3,4] has demanded more extensive studies in BAT metabolism. BAT is the specialized form of adipose tissue; whose primary function is for the dissipation of chemical energy into heat by the process called non-shivering thermogenesis[2]. This is enabled by its richness in mitochondria and uncoupling protein 1 (UCP1). BAT thermogenesis is usually escalated by cold-induced sympathetic activation, the neuronal release of noradrenaline (NA), and its subsequent β3 adrenergic signaling. Accumulating evidence in both animals and humans indicates that the thermogenic endowment of BAT plays a vital role in whole-body energy expenditure, metabolic homeostasis, and substrate utilization[5–7]. When fully activated, BAT can be regarded as a crucial metabolic sink for clearance of glucose, triglycerides, and other specific metabolites from circulation. This lead to lowered glucose and lipid levels and enhanced energy expenditure[8,9]. Therefore, identifying the upstream regulators of UCP1 in BAT becomes critical for developing BAT-targeted therapies for obesity and diabetes.

Reactive oxygen species (ROS), such as superoxide anions ($O_2^-$), hydrogen peroxide ($H_2O_2$), and hydroxyl radicals ($OH^•$), are the byproducts of cellular respiration under aerobic conditions. Electron leakage during substrate oxidation through electron transport chains located in the inner mitochondrial membrane produces a substantial amount of ROS within the mitochondria. Immediately after synthesis,

mitochondrial superoxide is dismutated to less reactive $H_2O_2$ by superoxide dismutase 2 (SOD2) in the mitochondrial matrix[10]. The $H_2O_2$ is further converted into non-reactive metabolic products by selenium-dependent antioxidant enzymes such as glutathione peroxidases (GPx), especially GPx1 and GPx4 present in the mitochondrial matrix and intermembrane space, respectively[11].

Although ROS are often described to be deleterious to various macromolecules, they also act as critical signaling molecules to provoke particular beneficial cellular adaptation in response to various stress conditions[12]. Notably, ROS increase mitochondrial proton conductance by activating mitochondrial UCPs, which may be a mechanism for decreasing the ROS concentrations inside mitochondria[13]. Chouchani et al.[14] reported that acute activation of brown adipose tissues substantially accompanies the mitochondrial ROS formation, which in turn alters redox status of the cysteine 253 thiol residue of UCP1 protein, resulting in increased NA sensitivity and accelerated thermogenesis. Furthermore, antioxidant sentrin2 overexpression in adipose tissues inhibits both basal and cold-induced UCP1 expressions, compromising thermogenesis in mice[15]. Conversely, adipose tissues specific deletion of the antioxidant enzyme, SOD2, protects the animals from diet-induced obesity by activating mitochondrial thermogenesis[16]. Taken together, we consider that ROS may activate thermogenesis either by direct redox modification of UCP1 or by altering the thermogenic gene expression.

Selenoprotein P, denoted as SeP (in humans, encoded by *SELENOP*, which was previously known as *SEPP1*), is a hepatokine, whose primary function is the antioxidation or redox regulation either by its direct enzymatic action or by supplying selenium to various cells for the synthesis of other selenoproteins[17,18]. Although the liver is the main contributor to circulating SeP[19], many other tissues locally synthesize SeP to some extent[20]. Previous studies have reported that SeP causes the pathology of type 2 diabetes, such as insulin resistance in the liver and skeletal muscle[21], hypo-adiponectinemia[22], impaired angiogenesis[23], insulin secretory failure in the pancreatic beta cells[24], exercise resistance in the skeletal muscle[25], and exacerbation of myocardial infarction[26]. Physiological ROS are required for cellular signal transduction, whereas excessive ROS-mediated oxidative stress causes diseases. SeP eliminates the physiological ROS burst required for intracellular signal transduction and thereby causes various signal resistance, the condition of which may be referred to as “reductive stress”[12].

Unexpectedly, our previous study revealed that *Selenop*-deficient mice have higher basal energy expenditure under a high-fat, high-sucrose diet[21], indicating the accelerated thermogenesis by *Selenop* deficiency. We hypothesized that the antioxidant action of SeP might impair BAT thermogenesis by interfering with the cold-induced mitochondrial ROS formation and its subsequent signaling. This study investigated the role of SeP in the cold- and NA-induced mitochondrial ROS formation, UCP1 activation, and thermogenesis in the brown adipose tissue. We present the evidence of previously under-recognized reductive stress in energy homeostasis. SeP may be an intrinsic factor inducing reductive stress that may be a potential therapeutic target for obesity and diabetes.

# Results

### Serum levels of SeP predict impaired BAT activity in humans

We previously observed that *Selenop*-deficient mice have higher basal energy expenditure under a high-fat, high-sucrose diet[21], which led us to hypothesize that SeP might impair the BAT activity. To confirm this hypothesis in humans, we assayed serum levels of SeP and investigated their association with BAT activity. After a mild cold exposure at 19°C for 2 hours, 87 non-diabetic healthy male subjects were evaluated for BAT activity using a positron emission tomography. In subjects who displayed higher BAT activity with SUVmax over 3, which is the median of the subjects, there was a significant negative correlation between serum SeP levels and BAT activity, suggesting the physiological function of SeP in heat generation (Fig. 1a).

### Deficiency of *Selenop* enhances UCP1 oxidation and thermogenesis in mice

To investigate the role of SeP in adaptive thermogenesis, we examined the systemic *Selenop* deficient mice under acute cold exposure at 4°C for 2 hours after overnight fasting. Following acute cold exposure, the BAT and rectal temperatures of the systemic *Selenop*-deficient mice were higher with lower post-exposure blood glucose levels than WT littermates (Fig. 1b-d). There were no differences in sympathetic actions such as urinary noradrenaline, serum FFA, and shivering between the genotypes (Supplementary Fig. 1a-c). However, the oxygen consumption rate (OCR) after 10 minutes of NA stimulation was significantly higher in the systemic *Selenop*-deficient mice than WT littermates (Fig. 1e). Therefore, systemic *Selenop*-deficient mice have a higher sensitivity to NA in their brown adipose tissues.

Next, we addressed whether reduced antioxidant capacity related to the phenotype of systemic *Selenop*-deficient mice. We treated mice with antioxidant N-acetyl cysteine (NAC) at a dose of 1.25 mmol/kg body weight for 6 hours before the cold exposure. The NAC pretreatment completely canceled the cold tolerant and glucose tolerant phenotypes of systemic *Selenop*-deficient mice (Fig. 1f-h). Indeed, BAT of systemic *Selenop*-deficient mice tended to be higher in the oxidative stress marker, thiobarbituric acid reactive substances (TBARS) than that of WT littermates after acute cold exposure (Fig. 1i). Because ROS are responsible for sulfenylation and activation of UCP1 protein[14], we evaluated the UCP1 sulfenylation status in the BAT of mice. BAT of systemic *Selenop*-deficient mice showed higher accumulation of sulfenylated UCP1 under cold exposure, which was entirely abolished by NAC pretreatment (Fig. 1j, k). There was no significant difference in the *Ucp1* mRNA level of BAT between genotypes (Fig. 1l). These findings suggest that SeP suppresses adaptive thermogenesis by eliminating ROS required for sulfenylation and activation of UCP1 without altering *Ucp1* expression in BAT.

### SeP suppresses noradrenaline-induced ROS generation, thermogenesis, and glucose uptake in brown adipocytes

To investigate the detailed mechanisms underlying the impaired thermogenesis by SeP in BAT, we treated primary brown adipocytes with purified human SeP (hSeP) protein. First, we evaluated hSeP action on redox status during NA-stimulation. Whole-cell ROS indicator, **Dihydroethidium (**DHE), revealed NA

treatment elevated ROS generation in the primary brown adipocytes, which was canceled by hSeP pretreatment (Fig. 2a). hSeP administration elevated the protein level of GPx4, which is known for mitochondrial form, but not GPx1 and selenoprotein W, in the primary brown adipocytes (Fig. 2b). OXPHOS complex II was reported to be the source of NA-induced ROS[25]. Indeed, complex II inhibitor (TTFA) and complex III inhibitor (Antimycin A) suppressed the NA-induced ROS generation (Fig. 2c), which confirmed the mitochondrial OXPHOS origin of NA-induced ROS generation. Thus, we focused on mitochondria-derived ROS as the target of SeP. Same as the results from whole-cell ROS status, NA stimulated mitochondrial ROS generation, which was abolished by hSeP pretreatment (Fig. 2d). We then assessed SeP action on heat generation in primary brown adipocytes using a cellular thermoprobe, a cationic fluorescent polymeric thermometer for measuring intracellular temperature[27]. NA administration stimulated primary brown adipocyte thermogenesis up to 3% (or 0.8℃ as converted value), whereas hSeP pretreatment completely canceled it (Fig. 2e and 2f). The hSeP pretreatment also canceled the NA-induced glucose uptake to primary brown adipocytes (Fig. 2g). The hSeP-mediated suppression of glucose uptake was associated with reduced phosphorylation of AMPK and mTOR (Fig. 2h).

We previously identified LDL receptor-related protein 1 (LRP1) as the SeP receptor in the skeletal muscle[25]. Also, it was reported that LRP8 is the SeP receptor in the brain[28] and testis[29] and that LRP2 is the receptor in the kidney[30]. Therefore, we hypothesized that one of the LDL receptor family members act as the SeP receptor in BAT. Among LDL receptor family members, Lrp1 was expressed predominantly in mouse BAT (Fig. 2i). The knockdown of Lrp1 in primary brown adipocytes almost entirely reduced hSeP uptake into the cells (Fig. 2j). These findings indicate that LRP1 is a functional and physiological receptor for SeP in BAT.

To confirm the intracellular effector of SeP, we performed the *Gpx1* and *Gpx4* knockdown in the primary brown adipocytes. The knockdown of *Gpx4*, but not *Gpx1*, rescued the hSeP-induced impairment of the NA-induced ROS production in the primary brown adipocytes (Fig. 2k). Additionally, pretreatment of the cells with the selective GPx4 inhibitor 1S, 3R RSL3 at 1 nM concentration for 1 hour enhanced the NA-induced thermogenesis of primary brown adipocytes (Fig. 2l and m). These findings indicate that SeP is uptaken into the brown adipocytes via its receptor Lrp1, upregulates GPx4 that eliminates the NA-induced generation of ROS, and thereby induces the resistance to the NA-induced thermogenesis and glucose uptake in the primary brown adipocytes.

### Deficiency of *Selenop* in the brown fat, but not in the liver, induces cold resistance in mice

Although the liver is a major SeP producing organ, we found that BAT also expresses the *Selenop* gene to some extent (Fig. 3a). To identify the primary source of SeP responsible for impaired BAT thermogenesis, we generated the liver-specific *Selenop*-deficient (L-*Selenop* KO) mice using *Alb-Cre* and BAT-specific *Selenop*-deficient (BAT-*Selenop* KO) mice using *Ucp1-Cre* (Supplementary Fig. 2a, b). Unexpectedly, no difference was seen in the rectal temperature during acute cold exposure between the L-*Selenop* KO mouse and the floxed mice (Fig. 3b). On the other hand, the rectal temperature tended to be higher in the BAT-*Selenop* KO mouse than the floxed mice during acute cold exposure (Fig. 3c).

To mimic the cold-induced thermogenesis, we measured the BAT and rectal temperatures directly during 0.2 mg/kg subcutaneous NA injection. After NA injection, the BAT-*Selenop* KO mice showed higher BAT and rectal temperatures compared with the floxed mice fed a normal chow (Fig. 3d and e). To estimate the impact of upregulated liver-derived SeP on thermogenesis in diet-induced obesity, we challenged a high-fat/high-sucrose (HFHS) diet for 16 weeks to the BAT-*Selenop* KO mice. HFHS diet feeding upregulated *Selenop* mRNA expression in the liver, but not in the BAT and other tissues, compared with normal chow feeding (Fig. 3f). As a result, HFHS diet feeding elevated serum levels of SeP, which were equivalent between the BAT-*Selenop* KO and the floxed mice, possibly due to the overproduction of SeP by the liver (Fig. 3g). The HFHS diet feeding canceled the enhanced NA-induced thermogenesis in the BAT-*Selenop* KO mice (Fig. 3h and i), suggesting the role of the liver-derived SeP in impaired BAT thermogenesis. These findings indicate that the locally produced SeP and the liver-derived SeP impair BAT thermogenesis under the normal chow and the HFHS diet, respectively.

We then investigated the molecular signature in the BAT and liver tissues after cold exposure at 4°C for 2 days. After cold exposure, the *Selenop* expression was significantly decreased in BAT but not in the liver (Fig. 3j). Additionally, NA stimulation reduced the expression of both *Selenop* and *Gpx4* in primary brown adipocytes (Fig. 3k). Treatment with an adenylate cyclase activator forskolin (10 μM for 24 hours) that mimics the NA action also showed similar results in primary brown adipocytes (Fig. 3l), but not in primary hepatocytes (Supplementary Fig. 3). These results indicate that the regulation of *Selenop* gene expression is variable among organs. Cold exposure and the NA stimulation downregulate *Selenop* specifically in BAT, which might be an adaptation to cold stress to enhance thermogenesis.

### Locally circulating SeP suppresses noradrenaline-induced ROS generation and thermogenesis in brown adipocytes

We found that the genes involved in selenoprotein family members, such as *Selenop*, *Gpx1*, *Gpx4*, and *Selenow*, were expressed in the primary brown adipocytes (Fig. 4a). To further confirm the role of locally expressed *Selenop* in BAT, we examined the *Selenop*-deficient primary brown adipocytes differentiated from the stromal vascular fraction (SVF) cells of systemic *Selenop*-deficient mice. The *Selenop*-deficient primary brown adipocytes showed higher NA-induced ROS production and thermogenesis than the control brown adipocytes (Fig. 4b, c, and d). Interestingly, pretreatment of brown adipocytes with sodium selenite abolished enhanced NA-induced ROS generation and thermogenesis in the *Selenop*-deficient primary brown adipocytes (Fig. 4e, f, and g). Finally, we investigated the significance of SeP in selenium-induced toxicity in BAT. The *Selenop*-deficient primary brown adipocytes showed intolerance to higher concentrations of selenium exposure (Fig. 4h), suggesting that SeP protects BAT from selenium toxicity by buffering excess selenium exposure.

## Discussions

In the current study, we found that SeP derived from BAT, rather than the liver, principally impairs BAT thermogenesis and glucose tolerance during physiological cold exposure or NA stimulation in mice. Remarkably, the regulation of *Selenop* expression is varied between BAT and liver in mice. Cold exposure

and NA signaling downregulate *Selenop* expression in BAT but not in the liver. On the other hand, the HFHS diet challenge to mice upregulates *Selenop* expression in the liver but not in BAT. These findings suggest that *Selenop* expression is locally regulated and plays a specific role in each organ. BAT may downregulate endogenous *Selenop* expression and elevate the NA sensitization in response to cold exposure. It is worth noting that HFHS diet feeding, which upregulates hepatic expression of *Selenop*, canceled the enhanced NA-induced BAT thermogenesis in BAT-*Selenop* KO mice. This result suggests the contribution of the liver-derived SeP overproduction to lower BAT activity in diet-induced obesity. Indeed, the higher serum levels of SeP, the lower the BAT activity in humans. These findings indicate that the locally produced SeP and the liver-derived SeP impair BAT thermogenesis under the normal chow and the HFHS diet, respectively. Therefore, it might be possible that SeP derived from both liver and BAT is a therapeutic target against obesity and type 2 diabetes.

Due to its high reactivity, ROS have been considered harmful as it oxidizes and damages various biomolecules. Indeed, lipid-induced excessive production of ROS mediates insulin resistance[31,32] and nonalcoholic steatohepatitis[33,34]. On the other hand, ROS transiently generated from NADPH oxidase enhances signal transduction via receptor tyrosine kinases by inactivating phosphatases such as PTP1B and PTEN[35]. We have previously found that SeP is overproduced in type 2 diabetic liver and causes various signal disturbances by eliminating intracellular physiological ROS required for signal transductions, the condition referred to as “reductive stress”[12]. Interestingly, there are a series of reports that an appropriate ROS stimulation activates UCP1 and enhances the heat production in BAT[14,36,37]. In the current study, we further proved that the SeP is involved in regulating BAT thermogenesis in mice by eliminating the mitochondrial ROS produced during NA signal transduction and thereby impairing UCP1 sulfenylation. To the best of our knowledge, SeP may be the first identified intrinsic factor inducing reductive stress that causes resistance to intracellular signal transduction.

SeP exerts antioxidative property directly through its selenocysteine residue and indirectly by supplying selenium to intracellular antioxidant GPx[38,39]. The present study identified GPx4, but not GPx1 and selenoprotein W, as the SeP-targeted downstream effector that inhibits the NA-induced mitochondrial ROS production and heat production in primary brown adipocytes. SeP may upregulate the mitochondria-localizing GPx4 that eliminates the NA-induced generation of ROS from mitochondria.

Selenium is an essential trace element but highly toxic at higher doses[40]. In the body, selenium mainly exists in incorporated form as selenoproteins[41]. We hypothesized that storing selenium in the form of SeP in the interstitial fluid is safer than storing free selenium intracellularly. In the present study, the *Selenop*-deficient primary brown adipocytes were intolerant to higher concentrations of selenium exposure. These findings suggest that locally expressed SeP protects BAT from selenium toxicity by buffering excess selenium. We identified Lrp1 as an uptake receptor for SeP in brown adipocytes. Collectively, we interpret that SeP is locally produced in BAT, pools selenium in the extracellular interstitial fluid, is uptaken via LRP1-mediated endocytosis, is transferred to the lysosome, supplies selenium into

the cells for the on-demand synthesis of GPx4, and thereby fine-tunes ROS-mediated excessive signal transduction.

Very recently, Jedrychowski, M. P. *et al.* reported that the selenited UCP1 with its 253rd cysteine replaced with selenium becomes redox-sensitive[42]. Dietary selenium supplementation in mice elevates energy expenditure through thermogenic adipose tissue and protects against obesity[42]. On the other hand, previous papers adduced that high serum selenium levels were positively associated with the prevalence of diabetes[43] and that long-term selenium supplementation for 200 μg/day increased the cumulative incidence of type 2 diabetes significantly[44]. These inconsistent findings may be associated with the epidemiological finding that the optimal blood range of selenium is narrow and non-linear in humans[42]. It may be challenging to maintain selenium levels in the exact sweet spot for health. At least in our present study, BAT-*Selenop* deficient mice showed enhanced NA-induced thermogenesis under standard selenium intake, which may not induce UCP1 selenation. Therefore, the current study highlights that SeP causes reductive stress to impair UCP1 activation and BAT thermogenesis in physiological conditions.

In conclusion, SeP-mediated reductive stress impairs cold-induced sulfenylation of UCP1, adaptive thermogenesis, and glucose uptake, the condition regarded as catecholamine resistance in BAT (Fig. 4i). SeP, as the hepatokine and BATkine, may be a therapeutic target to counter obesity and diabetes. Optimal regulation of excessive SeP may help convert excess energy to heat via manipulating BAT thermogenesis. To our knowledge, SeP may be the first identified intrinsic factor inducing reductive stress that causes resistance to intracellular signal transduction.

# Methods

### Human study

87 Japanese non-diabetic healthy male participants went to LSI Sapporo Clinic, Sapporo, Japan, for a complete physical examination. The subjects underwent the $^{18}$FDG-PET/CT scan procedure, as described previously[7,45]. After fasting for 6–12 h, the subjects entered an air-conditioned room at 19°C with light-clothing (usually a T-shirt with underwear) and put their legs on an ice block intermittently (usually for 4 min after every 5 min). One hour after the mild cold condition, they were given an intravenous injection of 259 megabecquerels (MBq) fluorodeoxyglucose (FDG) and maintained under the same cold conditions. One hour after the FDG injection, whole-body PET/CT scans were performed using a PET/CT system (Aquiduo; Toshiba Medical Systems, Tochigi, Japan) in a room at 24°C. With the CT parameters of 120 kV and real-exposure control, unenhanced low-dose spiral axial 2-mm collimated images were obtained. This was used for PET attenuation correction as well as anatomic localization. Subsequently, full-ring PET was performed in six incremental table positions, each ~15 cm in thickness. The total time for these scans was ~30 min.

PET and CT images were coregistered and analyzed using a VOX-BASE workstation (J-MAC System, Sapporo, Japan). Two experienced, blinded observers assessed the FDG uptake, particularly on both

sides of the neck and paravertebral regions, by visually judging the presence of radioactivity greater than that of the background. BAT activity in the neck region was quantified by calculating the maximal standardized uptake value ($SUV_{max}$), defined as the radioactivity per milliliter within the region of interest divided by the injected dose in megabecquerels per gram of body weight. Serum samples were obtained before $^{18}$FDG-PET/CT scan and used for the analysis of serum SeP level.

All participants provided written informed consent for participation in this study. All experimental protocols were approved by the Ethics Committees of Kanazawa University (approval no. 2017 − 158, UMIN000029276).

## Materials

The following antibodies were used as indicated dilutions. Rabbit anti-UCP1 polyclonal antibody (cat. no. #10983; 1:1,000), rabbit anti-GPX4 monoclonal antibody (cat. no. #125066; 1:1,000), rabbit anti-GPX1 polyclonal antibody (cat. no. # 22604; 1:1,000) and rabbit anti- LRP1 monoclonal antibody (cat. no. #92544; 1:20,000) were purchased from Abcam (Cambridge, UK). Rabbit anti-p38 MAPK polyclonal antibody (cat. no. #9212; 1:1,000), rabbit anti-phospho p38 MAPK (Thr180/Tyr182) polyclonal antibody (cat. no. #9211; 1:1,000), rabbit anti-total HSL polyclonal antibody (cat. no. #4107; 1:1,000), rabbit anti-phospho HSL (Ser660) polyclonal antibody (cat. no. #4126; 1:1,000), rabbit anti-phospho-AMPK (Thr172) monoclonal antibody (cat. no. #2535; 1:1,000), and rabbit anti-total-AMPK polyclonal antibody (cat. no. #2603; 1:1,000) and beta-actin antibodies (cat. no. #4967; 1:1,000) were purchased from Cell Signaling (Danvers, MA). Rabbit anti-selenoprotein W polyclonal antibody (cat. no. #600-401-A29) was purchased from Rockland (Limerick, Ireland). Rat anti-human selenoprotein P monoclonal antibody (BD-1) was made in house[46]. Collagenase D (Roche Diagnostics GmbH, cat. no. #11088866001), Dispase (Roche Diagnostics GmbH, cat. no. #04942078001), Indomethacin (Sigma-Aldrich, cat. no. #I7378), IBMX (Sigma-Aldrich, cat. no. #I5879), Dexamethasone (Sigma-Aldrich, cat. no. #D1756), rosiglitazone (Sigma-Aldrich, cat. no. #R2408), T3 (Sigma-Aldrich, cat. no. #T2877), Insulin (Sigma-Aldrich, cat. no. #I9278), Methoxypolyethylene glycol maleimide (PEG-Mal) (Sigma-Aldrich, cat. no. #63187), L-norepinephrine hydrochloride (Sigma-Aldrich, cat. no. #74480), N-ethyl maleimide (Wako, cat. no. #054-02063), TECP (Thermo Scientific, cat. no. #77720), N-acetyl cysteine (Sigma-Aldrich, cat. no. #A9165), 1S 3R-RSL3 (Sigma-Aldrich, cat. no. #SML2234) and phloretin (Wako, cat. no. #160-17781) were used.

## Animals

*Selenop*-deficient mice were produced by homologous recombination using genomic DNA cloned from an Sv-129 P1 library, as described previously[47]. BAT or Liver *Selenop*-deficient mice were maintained on a mixed B6/129 background. Mice carrying floxed alleles of *Selenop* (C57Bl/6 and 129/sv background) were originally obtained from R. F. Burk (Vanderbilt University School)[48]. Mice transgenically expressing Cre recombinase under the albumin promoter were generous gifts from Hiroshi Inoue (Kanazawa University). Mice transgenically expressing Cre recombinase under the *Ucp1* promoter were purchased from The Jackson Laboratory (J:206508). We backcrossed them with C57Bl/6 mice more than five times. Liver *Selenop*-KO mice were generated by crossing *Selenop* floxed mice with *Alb-Cre* transgenic mice. BAT

*Selenop*-KO mice were generated by crossing *Selenop* floxed mice with *Ucp1-Cre* transgenic mice. Because *Alb-Cre* transgenic mice or *Ucp1-Cre* transgenic mice and *Selenop*$^{fl/fl}$ mice were phenotypically indistinguishable, *Selenop*$^{fl/fl}$ mice were used as negative controls. All mice were genotyped by PCR using the following primers: 5'- TCCTAGATTGGCAGAGGATAGAATGAA – 3' and 5'-TCAGAAACACCTTCCAACTGTAATGC – 3' for the floxed Selenop gene and 5'-CGCCGCATAACCAGTGAAAC-3' and 5'-ATGTCCAATTTACTGACCG-3' for the Cre transgene.

### Animals Care

All the animal studies were carried out following the Guidelines on the Care and Use of Laboratory Animals issued by Kanazawa University. The protocol was approved by the ethical committee of Kanazawa University (Approval NO. 153678). C57BL/6J mice were obtained from Sankyo Lab Service (Tokyo, Japan). The mice were fed a standard rodent food diet CRF1 that contains 0.45 mg/kg of selenium (Oriental Yeast, Tokyo, Japan) or 60% fat rodent food D12492 that contains 0.27 mg/kg of selenium (Research Diet, New Brunswick, USA). All mice used in the current study had a C57BL/6J genetic background. Because female mice had inconsistent phenotypes, only male mice were used in this study. The mice at the age of 7–21 weeks were used unless otherwise indicated.

### Cold exposure and rectal temperature measurement

Six hours before cold exposure, all mice have fasted and injected intraperitoneally with PBS or NAC (1.25 mmol/kg body weight). A pair of WT and *Selenop*-deficient mice were put into a cage in the cold chamber at 4°C for 2 hours. Rectal temperatures were measured every 30 minutes during the period of cold exposure by using a rectal thermometer (weighing environment logger (AD-1687) & an endorectal probe for mice (AX-KO4746-100); A&D Company Limited, Tokyo, Japan). Shivering activities were assessed by video recording and manual counting at indicated time points during cold exposure. Blood glucose levels were measured before and after cold exposure by using a handheld blood glucose meter Glutest mint (Sanwa Kagaku Kenkyusho Co. Ltd., Nagoya, Japan). Serum Non-esterified fatty acid (NEFA) levels were determined by using the NEFA C Enzymatic assay kit (FUJIFILM Wako Diagnostics, USA), according to the manufacturer's instructions. Immediately after the completion of cold exposure, the mice were sacrificed to obtain tissue samples. For urinary norepinephrine measurement, 24-hour urine samples were collected while the mice were housing at the assigned temperature. Hydrochloric acid was added into the urine sample to a final concentration of 0.1 M for the integrity of norepinephrine until analysis. Urinary norepinephrine levels were measured by Norepinephrine ELISA Kit (Abnova Corporation, Taipei, Taiwan), according to the manufacturer's instructions. Urinary norepinephrine levels were normalized by creatinine content measured by the Creatinine colorimetric assay (Exocell, Philadelphia, PA).

### Image of interscapular temperature by a thermal camera in mice

The image of mice interscapular temperature was captured using the InfRec G100EX thermal camera (Nippon Avionics, Japan) after 2 hours of cold exposure at 4°C. All the mice were fasted for 6 hours before putting into the cold chamber.

### Oxygen consumption rate in mice

Six hours before the OCR measurement, all mice were fasted and injected intraperitoneally with PBS or NAC (1.25 mmol/kg body weight). After that, mice were anesthetized and put in an indirect calorimeter chamber individually (Oxymax; Columbus Instruments, Columbus, OH). After recording the baseline OCR for 30 min, the NA (1 mg/kg body weight) was injected subcutaneously and continued the recording for 44 min. $VO_2$ was measured every 8 or 10 minutes throughout the experiment. All procedures were performed under room temperature (24–26°C).

### Thiobarbituric acid reactive substances (TBARS)

Levels of TBARS in brown adipose tissue of mice were measured by using TBARS Assay Kit (Cayman Chemical) according to the manufacturer's instructions.

### BAT and rectal temperature measurements

BAT and rectal temperature under the NA stimulation in mice was measured according to a procedure previously described[49]. All mice were fasted in the thermoneutral chamber (30°C) for 12 hours before the experiment. All mice were anesthetized and kept on the heating plate. The sensor probes were inserted under the interscapular brown adipose tissues and in the rectum of the mice. The BAT and rectal temperatures were recorded by the multi-point temperature logger system (LT-200SA-TB, Tateyama Science High Technologies Co., Ltd.). At 5-min after starting temperature recording, the NA (0.2 mg/kg body weight) was injected subcutaneously and the temperature was recorded for 30 min.

### RNA isolation, cDNA synthesis, and real-time PCR analysis

Total RNA isolation, cDNA synthesis, and real-time PCR analysis were performed as previously described[50]. Quantitative RT-PCR was performed using TaqMan probes (Actb 4352341E; Gapdh 4352339E; 18S rRNA 4319413E; Sepp1 Mm00486048_m1; Lrp1 Mm00464608_m1; Ldlr Mm01177349_m1; Lrp2 Mm01328171_m1; Lrp8 Mm00474030_g1; Gpx1 Mm00656767_m1; Gpx4 Mm00515041_m1; Ucp1 Mm01244861_m1; Sepw1 Mm01268252_m1) and the StepOne Plus real-time PCR system (Life Technologies Corporation, Carlsbad, CA).

### ELISA for mouse SeP

Ninety-six- well microtiter plates were coated for 18 hr at 4°C with 100 µl of a coating antibody against mouse SeP (made in house) in 0.05 M sodium bicarbonate buffer, pH 9.6. The wells were washed four times with 200 µl PBS containing 0.05% Tween 20 (PBS/T) and incubated at 37°C with 150 µl of blocking solution (1 mg/ml BSA in PBS) for 1 hr. After washing the wells four times, 50 µl of plasma sample (diluted 50 times with PBS/T, containing 1 mg/ml BSA) was added to each well and incubated at 37°C for 1 hr. After washing the wells four times, 50 µl of 9S4 antibody for mouse SeP (Developmental Studies Hybridoma Bank deposited by Burke, R.D., RRID: AB_2617215) labeled with the Peroxidase Labeling Kit-NH2 (DONJINDO Molecular Technologies, Kumamoto, Japan) was added and incubated at 37°C for 1 hr. Finally, the plates were washed eight times. Fifty microliters of TMB was added to each well, and the enzyme-substrate reaction was allowed to proceed for 30 min at room temperature. The color development was stopped by adding 50 µl of 0.25 mol/L sulphuric acid, and the absorbance at 450 nm

was measured immediately. Because there are no commercially available mouse SeP protein standards, we compared the net value of absorbance.

### Western blot studies

We performed western blotting, as previously reported[25]. Densitometric analysis of blotted membranes was performed using Image Lab software (Bio-Rad Laboratories, Inc.).

### Assessment of sulfenylated UCP1 by gel shift

Sulfenylated UCP1 status in brown adipose tissues was measured as described previously[14]. In brief, mice BATs were isolated rapidly after indicated in vivo intervention and then homogenized in 100 nM NEM, 1 mM EGTA, 50 nM Tris-HCl, pH 7.4. Following incubation at 37°C for 5 min, the homogenate was further incubated with SDS (2% final) at 37°C for 10 min. Those incubation steps were performed by a thermomixer at 1,300 rpm. After that, excess NEM in the samples was removed by acetone precipitation. The pellets were then resuspended with 1 mM EGTA, 2% SDS, 10 mM TCEP, 50 mM Tris-HCl, pH 7.4 containing a 50 mM of polyethylene glycol polymer conjugated to maleimide (PEG-Mal). Resuspended samples were incubated at 37°C for 30 min, followed by second acetone precipitation to remove excess PEG-Mal. After resuspension of the pallet in RIPA lysis buffer, insolubilized debris was removed by centrifuging at 15,000 rpm for 30 minutes at 4°C. The supernatants were subjected to immunodetection by using the rabbit anti-UCP1 antibody.

### Purification of SeP

SeP was purified from human plasma using conventional chromatographic methods, as previously described[38]. Homogeneity of purified human SeP was confirmed by analysis of both amino acid composition and sequence[38].

### Primary brown adipocytes

Preparation and culture of primary brown adipocyte were performed as previously reported[51]. For the knockdown of the target gene, completely differentiated primary brown adipocytes were transfected with a 50 nM of indicated siRNA duplex oligonucleotides with Lipofectamine RNAiMAX (Invitrogen), using the reverse transfection method as described previously[52]. *Selenop* specific siRNA (Cat. no. #MSS208936), *Gpx1* specific siRNA (Cat. no. #MSS274652), *Gpx4* specific siRNA (Cat. no. #MSS286702), *Lrp1* specific siRNA (Cat. no. #NM008512.2), and negative control siRNAs were purchased from Invitrogen. siRNA transfection was performed for 48 hours, which was followed by the indicated intervention.

### Measurement of DHE oxidation

ROS production in primary brown adipocytes was measured by the DHE oxidation method. In brief, primary brown adipocytes were plated and differentiated in clear bottom black wall 96-well plates. After completion of differentiation, the culture medium was aspirated, and the cells were washed with imaging buffer (156 mM NaCl, 3 mM KCl, 1.25 mM $KH_2PO_4$, 2 mM $MgCl_2$, 10 mM HEPES, pH 7.4) two times. It was then replaced with fresh imaging buffer containing 1mM sodium pyruvate, 5 μM DHE (cat. no. #D23107, Invitrogen), and with or without 400 nM NA to detect NA-induced DHE oxidation. Fluorescence

intensity was measured at ex355/em460 for reduced DHE and ex544/em590 for oxidized DHE using a fluorescence plate reader (Glomax-Multi + Detection System, Promega). Oxidative stress levels in each sample were described as oxidized/reduced DHE at 30 min after NA stimulation, which were normalized by their respective baseline values.

### Measurement of mitochondrial ROS by MitoSOX assay

Measurement of mitochondrial specific superoxide levels was performed using MitoSOX red mitochondrial superoxide indicator (cat. no. #M36008, Invitrogen), as described by the manufacturer's instruction. Briefly, completely differentiated primary brown adipocytes were pretreated with or without 10 μg/ml SeP for 24 hours. After that, the cells were washed with PBS 3 times, and the culture medium was changed with phenol red-free DMEM/F12 supplemented with 5 μM MitoSOX with or without 1000 nM NA. Fluorescence intensity was measured at ex510/em580 at baseline and 30 min after NA stimulation. The mitochondrial ROS levels in each sample were described after normalization with their respective baseline values.

### Measurement of cellular temperature

NA-induced changes in intracellular temperature were measured in primary brown adipocytes by using Cellular Thermoprobe for Fluorescence Ratio (FDV-0005; Funakoshi, Tokyo, Japan). Primary brown adipocytes were cultured on glass-bottom dishes until fully confluent. The culture medium was then removed, and the cells were washed with a 5% glucose solution. 0.05% w/v of Cellular Thermoprobe in 5% glucose solution was then added to the cells, and the cultured dish was incubated at 25°C for 10 min. After washing with PBS three times, 100 μl of phenol red-free DMEM/F12 was added. For observation, excitation was carried out at 488 nm, and emission was monitored at 525 and 610 nm in a microscope cage incubation chamber at 37°C. Fluorescent ratio Em610/Em525 was used to evaluate temperature change. After recording baseline fluorescence intensity, the cells were stimulated with 400 nM NA (final concentration) or vehicle prepared in 100 μl of phenol red-free medium, followed by measurement of fluorescence intensity in a time-lapse manner. Fold changes in fluorescence intensity at each time point were calculated by normalization with baseline fluorescence intensity.

### Glucose uptake in brown adipocytes

Glucose uptake into primary brown adipocytes was assessed by using Glucose Uptake Cell-Based assay Kit (Cayman Chemical) according to the manufacturer's instruction. To describe in brief, after fully differentiation in 96 well plates, primary brown adipocytes were glucose and serum fasted in glucose-free DMEM (Gibco, Thermo Scientific) supplemented with 0.5% BSA for 6 hours. After that, cells were treated with glucose-free medium (with 0.5% BSA) containing 100 μg/ml 2-NBDG, 200 μM phloretin with or without 1000 nM NA for 5 minutes. At the end of the treatment, the plate was washed with ice-cold PBS 3 times to stop further glucose uptake into the cells. Then, 100 μl of Cell-Based Assay buffer was added to each well, and fluorescent intensity was measured at ex485/em535. Reading of the well treated with glucose-free medium without 2-NBDG treatment was regarded as blank.

### Statistical analyses

All data were analyzed using the Statistical Package for Social Science (SPSS) Version 21 advanced model and GraphPad Prism 8 software. Experimental data were visualized as box plots with individual points by a web tool, BoxPlotR[53]. Statistical methods were not used to determine sample size, but the sample size was chosen based on trial experiments or experiments performed previously. We randomized neither animals nor cell samples and performed all the experiments with blinding of the investigator. All groups in the current experiments showed normal variance. Statistical differences between two groups were assessed using unpaired two-tailed Student t-tests, except paired t-tests were used for blood glucose changes before and after cold exposure (Fig. 1d and g). Data involving more than two groups were assessed by analysis of variance (ANOVA) with Tukey's post hoc test. The AUC calculation and unpaired two-tailed Student t-tests were executed by GraphPad Prism 8 software (Fig. 2n, 3e, 3i, 4d, and 4f). By using the box-plot display tool in SPSS, we defined cases with values more than 3 times the interquartile range as outliers that were routinely excluded from all the analyses.

# Declarations

### COMPETING FINANCIAL INTERESTS

The authors declare no competing financial interests.

### AUTHOR CONTRIBUTIONS

H.T. and T.T. conceived the study and designed experiments. H.T., K-A.I., T.K., H.K.O., S.M.O., Y.S., Y.T., and M.M. conducted experiments. H.T., K-A.I., H.K.O., S.M.O., and T.T analyzed the data and provided the discussion. H.T., H.K.O., S.M.O., and T.T. wrote the manuscript with input from the other authors.


### ACKNOWLEDGMENTS

We thank M. Kawamura for technical assistance, Dr. H. Misu for useful discussion, and Prof. Shingo Kajimura, Prof, Edward T. Chouchani, and Prof. Bruce M. Spiegelman for methodological supports. We are indebted to K. E. Hill and R. F. Burk of Vanderbilt University School of Medicine for systemic *Selenop*-KO mice and *Selenop*$^{fl/fl}$ mice and to Hiroshi Inoue of Kanazawa University for *Alb-Cre* mice. This work was supported by the following grants: JSPS KAKENHI 18K16224 (H.T.) and 17H04199 (T.T.); MSD Life Science Foundation, Public Interest Incorporated Foundation (H.T.); Kato Memorial Bioscience Foundation (H.T.); Japan International Cooperation Agency (JICA) Project for Enhancement of Medical Education (J1410304, S.M.O.); MEXT Scholarship Program (Research student) for years 2019–2023 (H.K.O.); and JST Adaptable and Seamless Technology transfer Program (A-STEP) Grant Numbers AS2311400F and 15im0302407 (Y.S.).


# References


1. Saito, M. Brown adipose tissue as a therapeutic target for human obesity. *Obes. Res. Clin. Pract.* **7**, (2013).

2. Chouchani, E. T., Kazak, L. & Spiegelman, B. M. New Advances in Adaptive Thermogenesis: UCP1 and Beyond. *Cell Metab.* **29**, 27–37 (2019).
3. Cypess, A. M. *et al.* Identification and importance of brown adipose tissue in adult humans. *N. Engl. J. Med.* **360**, 1509–1517 (2009).
4. Van Marken Lichtenbelt, W. D. *et al.* Cold-activated brown adipose tissue in healthy men. *N. Engl. J. Med.* **360**, 1500–1508 (2009).
5. Stanford, K. I. *et al.* Brown adipose tissue regulates glucose homeostasis and insulin sensitivity. *J. Clin. Invest.* **123**, 215–223 (2013).
6. Lee, P., Greenfield, J. R., Ho, K. K. Y. & Fulham, M. J. A critical appraisal of the prevalence and metabolic significance of brown adipose tissue in adult humans. *Am. J. Physiol. - Endocrinol. Metab.* **299**, E601-606 (2010).
7. Yoneshiro, T. *et al.* Brown adipose tissue, whole-body energy expenditure, and thermogenesis in healthy adult men. *Obesity* **19**, 13–16 (2011).
8. Bartelt, A. *et al.* Brown adipose tissue activity controls triglyceride clearance. *Nat. Med.* **17**, 200–206 (2011).
9. Olsen, J. M. *et al.* β3-Adrenergically induced glucose uptake in brown adipose tissue is independent of UCP1 presence or activity: Mediation through the mTOR pathway. *Mol. Metab.* **6**, 611–619 (2017).
10. Miller, A. F. Superoxide dismutases: Ancient enzymes and new insights. *FEBS Lett.* **586**, 585–595 (2012).
11. Marí, M., Morales, A., Colell, A., García-Ruiz, C. & Fernández-Checa, J. C. Mitochondrial glutathione, a key survival antioxidant. *Antioxidants Redox Signal.* **11**, 2685–2700 (2009).
12. Takamura, T. Hepatokine selenoprotein P-mediated reductive stress causes resistance to intracellular signal transduction. *Antioxid. Redox Signal.* ars.2020.8087 (2020). doi:10.1089/ars.2020.8087
13. Echtay, K. S. *et al.* Superoxide activates mitochondrial uncoupling proteins. *Nature* **415**, 96–99 (2002).
14. Chouchani, E. T. *et al.* Mitochondrial ROS regulate thermogenic energy expenditure and sulfenylation of UCP1. *Nature* **532**, 112–116 (2016).
15. Ro, S.-H. *et al.* Sestrin2 inhibits uncoupling protein 1 expression through suppressing reactive oxygen species. *Proc. Natl. Acad. Sci.* **111**, 7849–7854 (2014).
16. Han, Y. H. *et al.* Adipocyte-specific deletion of manganese superoxide dismutase protects from diet-induced obesity through increased mitochondrial uncoupling and biogenesis. *Diabetes* **65**, 2639–2651 (2016).
17. Saito, Y. & Takahashi, K. Characterization of selenoprotein P as a selenium supply protein. *Eur. J. Biochem.* **269**, 5746–5751 (2002).
18. Burk, R. F. & Hill, K. E. Selenoprotein P-Expression, functions, and roles in mammals. *Biochim. Biophys. Acta - Gen. Subj.* **1790**, 1441–1447 (2009).

19. Schweizer, U. *et al.* Hepatically derived selenoprotein P is a key factor for kidney but not for brain selenium supply. *Biochem. J.* **386**, 221–226 (2005).
20. Hoffmann, P. R. *et al.* The selenoproteome exhibits widely varying, tissue-specific dependence on selenoprotein P for selenium supply. *Nucleic Acids Res.* **35**, 3963–3973 (2007).
21. Misu, H. *et al.* A liver-derived secretory protein, selenoprotein P, causes insulin resistance. *Cell Metab.* **12**, 483–495 (2010).
22. Misu, H. *et al.* Inverse correlation between serum levels of selenoprotein p and adiponectin in patients with type 2 diabetes. *PLoS One* **7**, e34952 (2012).
23. Ishikura, K. *et al.* Selenoprotein P as a diabetes-associated hepatokine that impairs angiogenesis by inducing VEGF resistance in vascular endothelial cells. *Diabetologia* **57**, 1968–1976 (2014).
24. Mita, Y. *et al.* Selenoprotein P-neutralizing antibodies improve insulin secretion and glucose sensitivity in type 2 diabetes mouse models. *Nat. Commun.* **8**, 1–17 (2017).
25. Misu, H. *et al.* Deficiency of the hepatokine selenoprotein P increases responsiveness to exercise in mice through upregulation of reactive oxygen species and AMP-activated protein kinase in muscle. *Nat. Med.* **23**, 508–516 (2017).
26. Chadani, H. *et al.* Endogenous selenoprotein P, a liver-derived secretory protein, mediates myocardial ischemia/reperfusion injury in mice. *Int. J. Mol. Sci.* **19**, (2018).
27. Uchiyama, S., Gota, C., Tsuji, T. & Inada, N. Intracellular temperature measurements with fluorescent polymeric thermometers. *Chem. Commun.* **53**, 10976–10992 (2017).
28. Burk, R. F. *et al.* Deletion of apolipoprotein E receptor-2 in mice lowers brain selenium and causes severe neurological dysfunction and death when a low-selenium diet is fed. *J. Neurosci.* **27**, 6207–6211 (2007).
29. Olson, G. E., Winfrey, V. P., NagDas, S. K., Hill, K. E. & Burk, R. F. Apolipoprotein E receptor-2 (ApoER2) mediates selenium uptake from selenoprotein P by the mouse testis. *J. Biol. Chem.* **282**, 12290–12297 (2007).
30. Olson, G. E., Winfrey, V. P., Hill, K. E. & Burk, R. F. Megalin mediates selenoprotein p uptake by kidney proximal tubule epithelial cells. *J. Biol. Chem.* **283**, 6854–6860 (2008).
31. Matsuzawa-Nagata, N. *et al.* Increased oxidative stress precedes the onset of high-fat diet–induced insulin resistance and obesity. *Metabolism* **57**, 1071–1077 (2008).
32. Nakamura, S. *et al.* Palmitate induces insulin resistance in H4IIEC3 hepatocytes through reactive oxygen species produced by mitochondria. *J. Biol. Chem.* **284**, 14809–14818 (2009).
33. Ota, T. *et al.* Insulin Resistance Accelerates a Dietary Rat Model of Nonalcoholic Steatohepatitis. *Gastroenterology* **132**, 282–293 (2007).
34. Matsuzawa, N. *et al.* Lipid-induced oxidative stress causes steatohepatitis in mice fed an atherogenic diet. *Hepatology* **46**, 1392–1403 (2007).
35. Chiarugi, P. & Cirri, P. Redox regulation of protein tyrosine phosphatases during receptor tyrosine kinase signal transduction. *Trends Biochem. Sci.* **28**, 509–514 (2003).

36. Chouchani, E. T., Kazak, L. & Spiegelman, B. M. Mitochondrial reactive oxygen species and adipose tissue thermogenesis: Bridging physiology and mechanisms. *J. Biol. Chem.* **292**, 16810–16816 (2017).
37. Mills, E. L. *et al.* Accumulation of succinate controls activation of adipose tissue thermogenesis. *Nature* **560**, 102–106 (2018).
38. Saito, Y. *et al.* Selenoprotein P in human plasma as an extracellular phospholipid hydroperoxide glutathione peroxidase: Isolation and enzymatic characterization of human selenoprotein P. *J. Biol. Chem.* **274**, 2866–2871 (1999).
39. Takebe, G. *et al.* A comparative study on the hydroperoxide and thiol specificity of the glutathione peroxidase family and selenoprotein P. *J. Biol. Chem.* **277**, 41254–41258 (2002).
40. MacFarquhar, J. K. Acute Selenium Toxicity Associated With a Dietary Supplement. *Arch. Intern. Med.* **170**, 256 (2010).
41. Yang, R., Liu, Y. & Zhou, Z. Selenium and Selenoproteins, from Structure, Function to Food Resource and Nutrition. *Food Sci. Technol. Res.* **23**, 363–373 (2017).
42. Jedrychowski, M. P. *et al.* Facultative protein selenation regulates redox sensitivity, adipose tissue thermogenesis, and obesity. *Proc. Natl. Acad. Sci. U. S. A.* **117**, 10789–10796 (2020).
43. Bleys, J., Navas-Acien, A. & Guallar, E. Serum Selenium and Diabetes in U.S. Adults. *Diabetes Care* **30**, 829–834 (2007).
44. Stranges, S. *et al.* Effects of long-term selenium supplementation on the incidence of type 2 diabetes: a randomized trial. *Ann. Intern. Med.* **147**, 217–23 (2007).
45. Saito, M. *et al.* High incidence of metabolically active brown adipose tissue in healthy adult humans: Effects of cold exposure and adiposity. *Diabetes* **58**, 1526–1531 (2009).
46. Saito, Y., Watanabe, Y., Saito, E., Honjoh, T. & Takahashi, K. Production and application of monoclonal antibodies to human selenoprotein P. *J. Heal. Sci.* **47**, 346–352 (2001).
47. Hill, K. E. *et al.* Deletion of selenoprotein P alters distribution of selenium in the mouse. *J. Biol. Chem.* **278**, 13640–13646 (2003).
48. Hill, K. E. *et al.* Production of selenoprotein P (Sepp1) by hepatocytes is central to selenium homeostasis. *J. Biol. Chem.* **287**, 40414–40424 (2012).
49. Inokuma, K. I. *et al.* Uncoupling protein 1 is necessary for norepinephrine-induced glucose utilization in brown adipose tissue. *Diabetes* **54**, 1385–1391 (2005).
50. Tajima-Shirasaki, N. *et al.* Eicosapentaenoic acid down-regulates expression of the selenoprotein P gene by inhibiting SREBP-1c protein independently of the AMP-activated protein kinase pathway in H4IIEC3 hepatocytes. *J. Biol. Chem.* **292**, 10791–10800 (2017).
51. Aune, U. L., Ruiz, L. & Kajimura, S. Isolation and differentiation of stromal vascular cells to beige/brite cells. *J. Vis. Exp.* (2013). doi:10.3791/50191
52. Isidor, M. S. *et al.* An siRNA-based method for efficient silencing of gene expression in mature brown adipocytes. *Adipocyte* **5**, 175–185 (2016).

53. Spitzer, M., Wildenhain, J., Rappsilber, J. & Tyers, M. BoxPlotR: A web tool for generation of box plots. *Nature Methods* **11**, 121–122 (2014).

# Figures

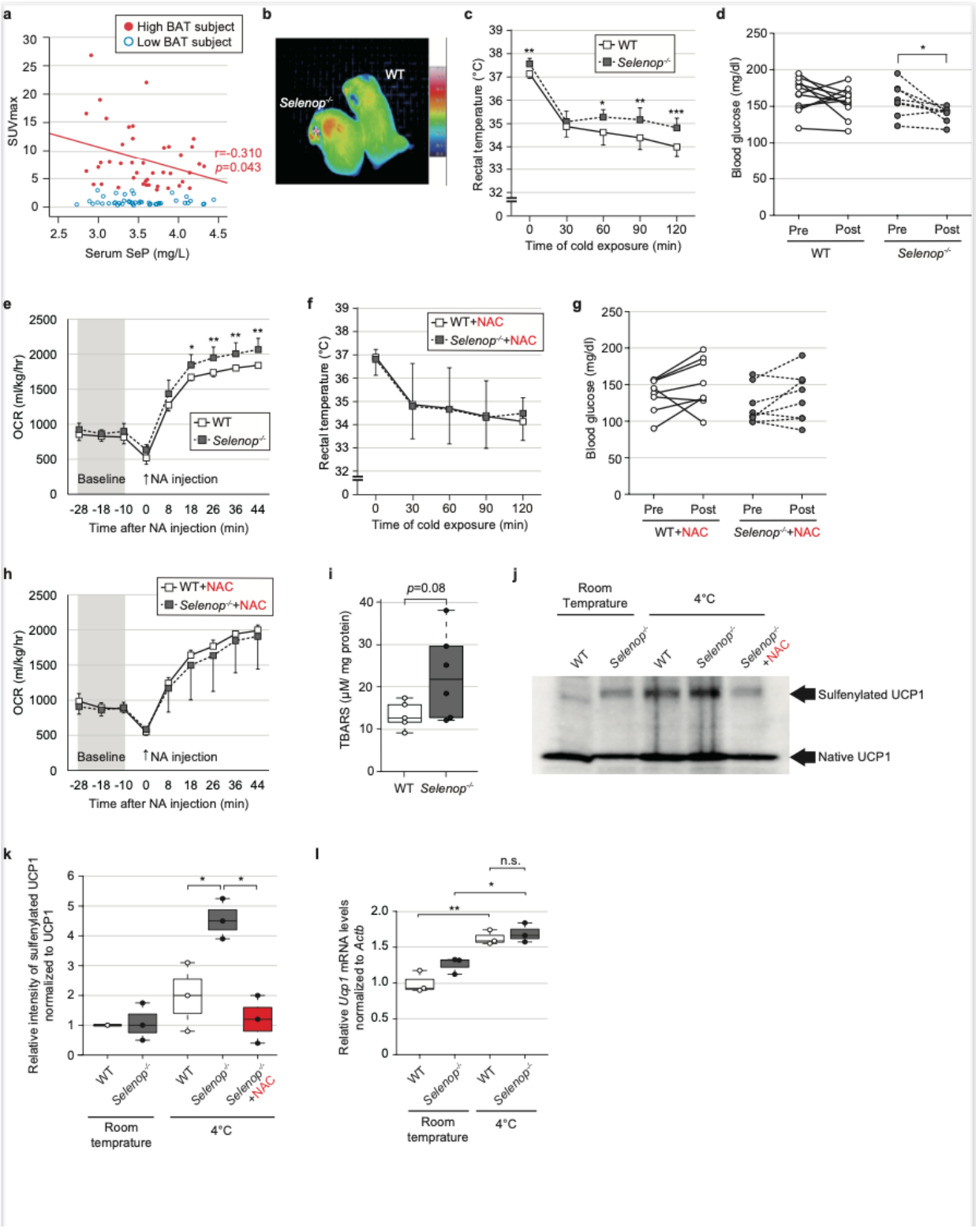


**Figure 1**

eficiency of Selenop enhances UCP1 sulfenylation and thermogenesis. (a) Scatter plot showing plasma SeP concentrations and brown aditpose tissue (BAT) activity in high BAT or low BAT activity groups of human subjects who were divided by SUVmax = 3, which is the median of the subjects (n = 43 subjects in high BAT, n = 44 subjects in low BAT). (b) Representative image of interscapular temperature by the thermal camera in wild-type (WT) and systemic Selenop-deficient mice after acute cold exposure. (c) The rectal temperature during acute cold exposure in WT and Selenop-deficient mice (n = 11 mice for WT; n = 8 mice for Selenop-/-). (d) Blood glucose levels before and after cold exposure in WT and systemic Selenop-deficient mice (n = 11 mice for WT; n = 8 mice for Selenop-/-). (e) Oxygen consumption rate (OCR) after noradrenaline stimulation in WT and systemic Selenop-deficient mice (n = 6 mice per group). (f) The rectal temperature during cold exposure in WT and systemic Selenop-deficient mice pretreated with N-acetylcysteine (NAC) for 6 hours (n = 8 mice per group). (g) Blood glucose levels before and after cold exposure in WT and systemic Selenop-deficient mice pretreated with NAC (n = 8 mice per group). (h) OCR after noradrenaline stimulation in WT and systemic Selenop-deficient mice pretreated with NAC (n = 4 mice for WT; n = 8 mice for Selenop-/-). (i) TBARS levels in brown fat of WT and systemic Selenop-deficient mice after cold exposure (n = 5 mice for WT; n = 6 mice for Selenop-/-). (j, k) Representative western blot images (j) and quantification (k) of UCP1 sulfenylation in the BAT of WT and systemic Selenop-deficient mice after cold exposure with or without NAC pretreatment (n = 3 mice per group). (l) Ucp1 gene expression in the BAT of WT and systemic Selenop-deficient mice after cold exposure (n = 8 mice per group). In box-plots (i, k, l), center lines show the medians, and box limits indicate the 25th and 75th percentiles; whiskers extend 1.5x the interquartile range from the 25th and 75th percentiles; data points are plotted as dots. In c, e, f, h, data are represented as mean ± SD. *P < 0.05; **P < 0.01; ***P < 0.001; n.s., not significant; by Pearson correlation (a); by two-tailed unpaired student’s t-test (c, e, f, h, i); by two-tailed paired student’s t-test (d, g); by one-way analysis of variance (ANOVA) with Tukey’s post hoc test (k, l). Full images are shown in Supplementary Figure 4.

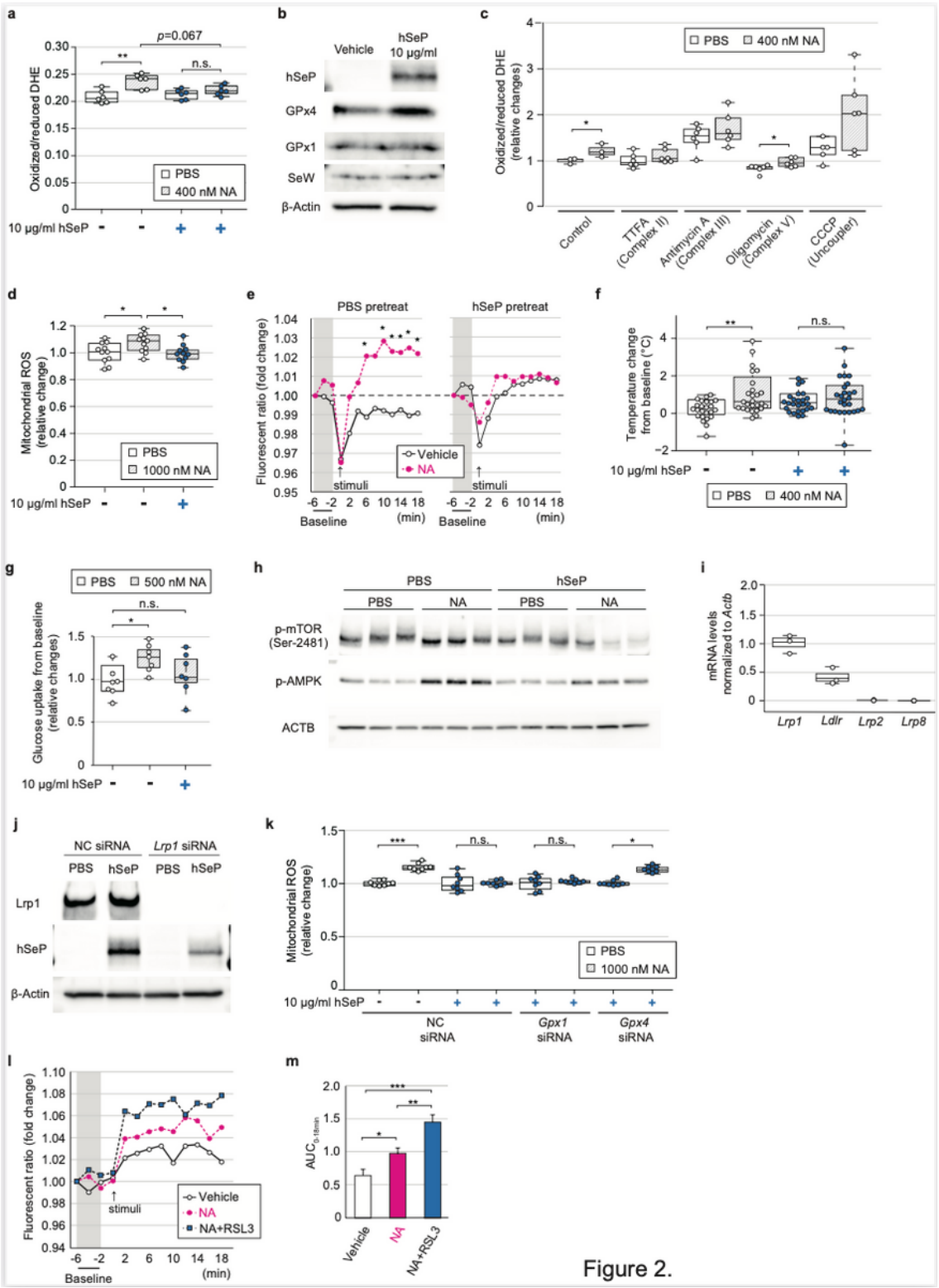


Figure 2.

## Figure 2

SeP suppresses noradrenaline-induced ROS generation, thermogenesis, and glucose uptake in brown adipocytes. Effects of hSeP on superoxide dependent oxidation of DHE (a, n = 6) and selenoproteins production in primary brown adipocytes (b). (c) Effects of OXPHOS inhibitors on NA-induced ROS generation (n = 6). Effects of hSeP on mitochondrial ROS generation (d, n= 11) and intracellular temperature (e, n = 23-27 cells each) in NA-stimulated primary brown adipocytes. (f) Maximum change of

intracellular temperature from baseline. The temperature difference between the highest after NA stimulation and baseline was calculated. (g) Effects of hSeP on glucose uptake in noradrenaline-stimulated primary brown adipocytes (n = 7 wells each). (h) Western blot images of phosphorylated mTOR and AMPK in NA-stimulated primary brown adipocytes pretreated with hSeP. (i) Gene expression levels of LDLR family members in primary brown adipocytes (n = 3 samples each). (j) Representative western blot images of hSeP uptake in Lrp1-knockdown primary brown adipocytes. (K) Effect of knockdown of Gpx1 or Gpx4 on hSeP induced inhibition of mitochondrial ROS production in NA-stimulated primary brown adipocytes (n = 8 wells in each group) (l and m) Effect of 1S, 3R RSL3 pretreatment on the cellular temperature of NA stimulated primary brown adipocytes (n = 50 cells in each group). Fold change of fluorescent ratio (l) and area under the curve (AUC) of 0 - 18 min (m). In box-plots (a, c, d, f, g, i, k), center lines show the medians, and box limits indicate the 25th and 75th percentiles; whiskers extend 1.5x the interquartile range from the 25th and 75th percentiles; data points are plotted as dots. In bar graph (m), data are represented as mean ± SEM. of biologically independent samples. *P < 0.05; **P < 0.01; ***P < 0.001; n.s., not significant by one-way ANOVA with Tukey’s post hoc test (a, c, f, g, l, n). Full images are shown in Supplementary Figure 5.

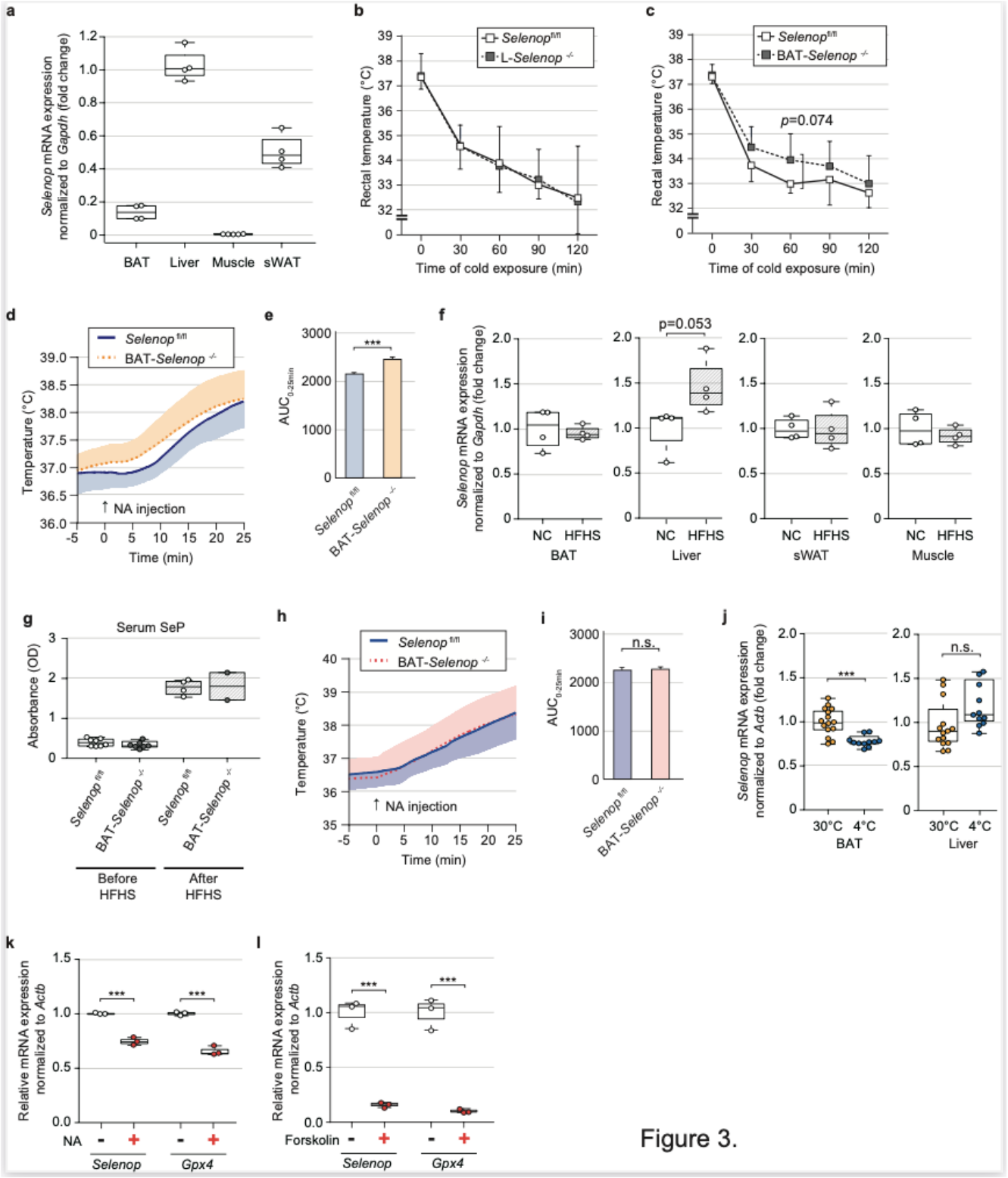


Figure 3.

## Figure 3

Deficiency of SELENOP in the brown fat, but not in the liver, induces cold resistance in mice. (a) Selenop mRNA expression in various tissues of C57BL/6J mice (n = 4-5 mice per group). (b) The rectal temperature during acute cold exposure in the liver-specific Selenop-deficient mice (n = 5 mice per group). (c) The rectal temperature during cold exposure in the BAT-specific Selenop-deficient mice (n = 7 mice per group). (d and e) BAT temperature after subcutaneous NA injection in the BAT-specific Selenop-deficient

mice (d; n = 8 mice per group) and AUC of 0 - 25 min (e). (f) Selenop expression in various tissues of C57BL/6J mice with or without HFHS feeding (n = 4 mice per group). (g) Circulating SeP levels before and after HFHS feeding. (h and i) BAT temperature after subcutaneous NA injection in the BAT-specific Selenop-deficient mice after HFHS feeding (h; n = 8 mice per group) and AUC of 0 - 25 min (i). (j) Selenop expression in BAT and liver tissue of WT mice after 2 days of chronic cold exposure at 4℃ (n = 12 mice in 4℃ group and 15 mice in 30℃ group). (k and l) Selenop and Gpx4 expression in primary brown adipocytes after NA treatment (k) and after forskolin treatment (l) (n = 3 per group). The 800 nM NA medium for 6 hours or the 10 uM forskolin medium for 24 hours were treated to fully differentiated primary brown adipocytes. In box-plots (a, f, g, j, k, l), center lines show the medians, and box limits indicate the 25th and 75th percentiles; whiskers extend 1.5x the interquartile range from the 25th and 75th percentiles; data points are plotted as dots. In b, c, d, h, data are represented as mean ± SD. In e, i, data are represented as mean ± SEM.*P < 0.05; **P < 0.01, ***P < 0.001; n.s., not significant by two-tailed unpaired student’s t-test (b, c, e, f, i, j, k, l). =

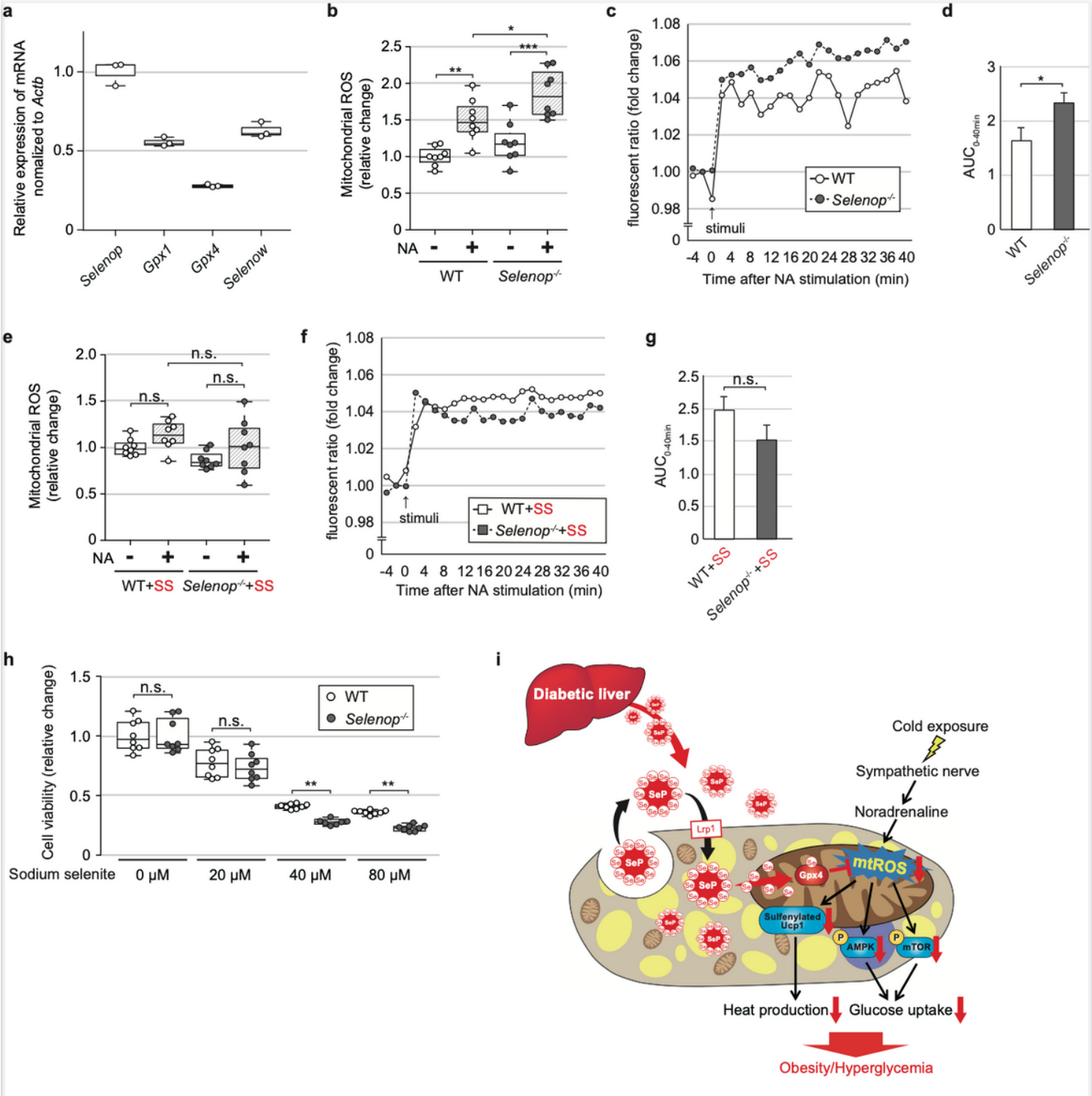


## Figure 4

Locally circulating SELENOP suppress noradrenaline-induced ROS generation and thermogenesis in brown adipocytes. (a) Gene expression of selenoprotein family in primary brown adipocytes (n = 3). (b - d) Effect of NA stimulation to WT and Selenop-deficient primary brown adipocytes on MitoSOX (b; n = 8 wells per group), cellular temperature (c; n = 50 cells per group), and AUC of 0 - 40 min (d). (e - g) Effect of NA stimulation to WT and Selenop-deficient primary brown adipocytes with sodium selenite pretreatment on MitoSOX (e; n = 8 wells per group), cellular temperature (f; n = 56 cells per group), and AUC of 0 - 40

min (g). The 5 uM sodium selenite medium and control medium were treated to fully differentiated primary brown adipocytes for 24 hours. After that, the cells used for the experiments. (h) Cell viability of primary brown adipocytes with various concentrations of sodium selenite treatment (n = 8 wells per group). (i) Schematic diagram depicting that the SeP blunts ROS-regulated thermogenesis in brown fat. In box-plots (a, b, e, h), center lines show the medians, and box limits indicate the 25th and 75th percentiles; whiskers extend 1.5x the interquartile range from the 25th and 75th percentiles; data points are plotted as dots. In d, g, data are represented as mean ± SEM.. *P < 0.05; **P < 0.01, ***P < 0.001; n.s., not significant; by one-way analysis of variance (ANOVA) with Tukey's post hoc test (b, e); by two-tailed unpaired student's t-test (d, g, h).

## Supplementary Files

This is a list of supplementary files associated with this preprint. Click to download.

- SupplementaryFig.1.eps
- SupplementaryFig.2.eps
- SupplementaryFig.3.eps
- SupplementaryFig.4.eps
- SupplementaryFig.5.eps